Workforce: status and needs

The software core team at CERN plays a pivotal role in driving and coordinating the majority of FCC activities. This team has evolved over time, initially as part of EP-SFT and now of the newly created EP-FCC group. The current workforce at CERN includes (in FTEs): 1.4 staff members, providing leadership and continuity; 3 fellows; 3 students (technical and doctoral). Additionally, the CERN EP RD program has been instrumental in providing fellow support, particularly for the development and advancement of Key4HEP, a critical component for the FCC activities. Contributions from external institutes have increased, in particular from collaborators in France, Italy, and United States. This expanding network of external contributors strengthens the FCC effort by bringing diverse expertise, resources, and perspectives, complementing the core team's efforts at CERN.

Consolidating and expanding the team is essential to sustain progress, address emerging challenges, and capitalize on synergies with other initiatives. To strengthen this team, efforts are being made to secure: 2 additional staff positions for long-term stability and expertise; 2 continued fellows to retain knowledge and maintain operational continuity; 2 technical students, providing critical support for development tasks and creating a pipeline for future talent. In addition a dedicated IT contact would be benificial to foster strong relationships with CERN IT service groups, ensure streamlined access to IT services and infrastructure critical to FCC activities.

Key4hep, the software ecosystem central to FCC workflows, requires ongoing development and maintenance. Establishing long-term support mechanisms will be crucial to ensure Key4hep's continued relevance and effectiveness. Discussions with CERN EP management are focused on securing the platform's future as it transitions from its current RD phase to a fully operational status.

Closer ties with the LHC community can unlock mutual benefits, by leveraging shared technologies that advance both FCC and LHC objectives. In this respect, promoting 50-50 shared positions might help to foster joint development efforts and enhance expertise exchange. Finally, To broaden the project's resource base, continued efforts are needed to attract more external contributors from institutes worldwide, raise awareness and interest in FCC among the broader scientific community, encouraging partnerships and resource sharing.

Outlook

The FCC PED studies will demand a significant expansion of both computing and human resources to achieve their objectives effectively. Meeting FCC's growing computational needs involves pursuing multiple avenues inspired by the LHC model, with integration into the WLCG resource pool, and leveraging HPC calls and exploring opportunistic usage of available resources. Continued efforts are required to optimize software frameworks and computational strategies, address challenges in physics analysis, and identify potential criticalities. Effective data storage and management remain critical, with retention policies possibly needed to maximize efficiency and ensure sustainability.

A preliminary look at the requirements for the Z run suggests that the computing demands for this phase should remain manageable within the current evolution of the current resources. This points to the viability of the project's computing strategy under realistic resource constraints. However, sustained efforts in resource optimization will be essential for maintaining this balance as the project progresses.

7.10 Outlook

8 Energy calibration, polarisation, monochromatisation

8.1 Overview

Excellent knowledge of the collision energy E_{CM} is vital for many of the most important measurements that will be performed at FCC-ee, in particular the determination of the Z-resonance parameters and the mass of the W boson. To achieve this goal requires calibrating the mean energy of each beam around the ring $\mathrm{E_b}$ (in principle not identical for electrons and positrons, but here designated with a single symbol for simplicity), and then applying corrections to the naive relation $\mathrm{E_{CM}} = 2\mathrm{E_b}$ to obtain the centre-of-mass energy at each interaction point.

Circular colliders have the unique attribute that transverse polarisation naturally accumulates through the Sokolov-Ternov effect, and the spin tune, which is the ratio of the precession frequency to the revolution frequency, is directly proportional to $\mathrm{E_b}$. The spin tune can be directly measured by the procedure of resonant depolarisation (RDP) in which the frequency of a depolariser kicker magnet is adjusted until the polarisation is found to vanish. This technique has been exploited at many facilities, most notably at LEP in scans of the Z resonance [701]. Alternatively, in a free spin precession (FSP) measurement the depolariser may be used to rotate the spin vector into the horizontal plane, and the precession frequency measured directly. These measurements, however, will only be possible for Z-pole operation and at energies up to and including the $\mathrm{W^+W^-}$ threshold. At higher energies than these, the polarisation level will be too small for RDP and FSP measurements to be practical, and the energy scale will have to be determined from physics processes at the experiments, such as $e^+e^- \to f\bar{f}(\gamma)$ production. Here, radiative returns to the Z-pole allow for a normalisation that then can be applied for non-radiative events at higher energies.

The calculation of $\mathrm{E_{CM}}$ at each interaction point requires good knowledge of the crossing angle of the two beams. In addition, it is necessary to account for local energy variations from synchrotron radiation, the RF system and impedance, and to consider the effects of opposite-sign vertical dispersion.

The knowledge of $\mathrm{E_b}$ at LEP was ultimately limited by the sampling rate of RDP measurements, which were performed outside physics operation with a periodicity of around a week. The energy was found to vary significantly between measurements due to several effects, for example earth tides [701]. In order to enable the much greater degree of systematic control that the vastly larger sample sizes at FCC-ee warrant, the operational strategy will be very different to LEP. Measurements of $\mathrm{E_b}$ will be performed several times an hour on non-colliding pilot bunches. In Z running, around 250 pilot bunches will be injected at start of fill, and wiggler magnets will be activated to speed up the polarisation time. One to two hours will be required for the polarisation to build, after which the wigglers will be turned off and physics (colliding) bunches injected. The RF frequency will be continually adjusted to keep the beams centred in the quadrupoles, thus suppressing tide-driven energy changes, which would otherwise be $\mathcal{O}$(100 MeV). A model will be developed to track residual energy variations between measurements.

Full discussion on the machine aspects concerning the $\mathrm{E_{CM}}$ calibration can be found in *insert cross-reference to accelerator volume, when known*. Here a summary is given of the contribution to these studies coming from the experiments, and the foreseen performance with the current level of understanding.

Also included below is a brief discussion of the studies that are underway for monochromatisation of the collision energy when operating at an $\mathrm{E_{CM}}$ of around 125 GeV, corresponding to the mass of the Higgs boson. This is motivated by the need to reduce the spread of $\mathrm{E_{CM}}$ to a value similar to that of the Higgs width (around 4 MeV), thereby improving the sensitivity to direct Higgs production and allowing tight constraints to be placed on the electron-Yukawa coupling constant.

8.2 Input from the experiments

The experiments operating at FCC-ee will themselves provide measurements that are vital input for the calibration of the collision energy and related quantities. A full discussion of these measurements can be found in Ref. [18]. Here, a brief summary is given, together with some recent updates.

The principal data set for performing these measurements is the very large sample of dimuon events that each experiment will collect, $i.e.$ those arising from the process $e^+e^- \to \mu^+\mu^-(\gamma)$, where (γ) indicates the possible presence of an initial-state photon. Analysis of the topology of these events allows several important quantities to be determined.

The crossing angle α

The nominal value of the crossing angle is $\alpha = 30$ mrad, but the true value must be determined throughout data-taking in order that the collision energy can be calculated to the required precision. At the Z pole, more than 10^6 dimuon events will be collected every 10 minutes, which will allow this parameter to be measured with a statistical uncertainty of 0.0003 mrad, which is sufficient for the physics goals, since a precision of 0.015 mrad leads to an uncertainty of 10 keV on $\mathrm{E_{CM}}$. The statistical precision will be worse at higher energies, where the production rate is lower, but will not compromise the physics measurements that are targeted in these regimes.

There is an important subtlety in the crossing-angle determination that must be accounted for. The electron and positron bunches experience mutual electric and magnetic fields that accelerate (decelerate) the bunches before (after) the collision, and also increase (decrease) the crossing angle. The collision energy is invariant, but the change in crossing angle from this effect (estimated to be a relative 0.6% modification) must be known so that the measured crossing angle can be corrected back to the unaffected quantity, and used together with beam energies as determined from RDP to calculate $\mathrm{E_{CM}}$.

The size of the change in α depends on parameters such as the bunch population and the spread in collision energy $\sigma_{\mathrm{E_{CM}}}$. It is found empirically from simulation studies that α is proportional to $\mathcal{L}^{1/2}/\sigma_{\mathrm{E_{CM}}}{}^{1/6}$. By measuring α and $\sigma_{\mathrm{E_{CM}}}$ for different bunch intensities it will be possible to extrapolate to zero intensity and determine the value of α in the absence of these effects. A good opportunity to perform these measurements would be in the period that top-up injection is taking place. It is therefore important that conditions allow detector operation during this period, and that the beams are stable. A simulated study of the measurement of α against $\mathcal{L}^{1/2}/\sigma_{\mathrm{E_{CM}}}{}^{1/6}$ is presented in Fig. 125.

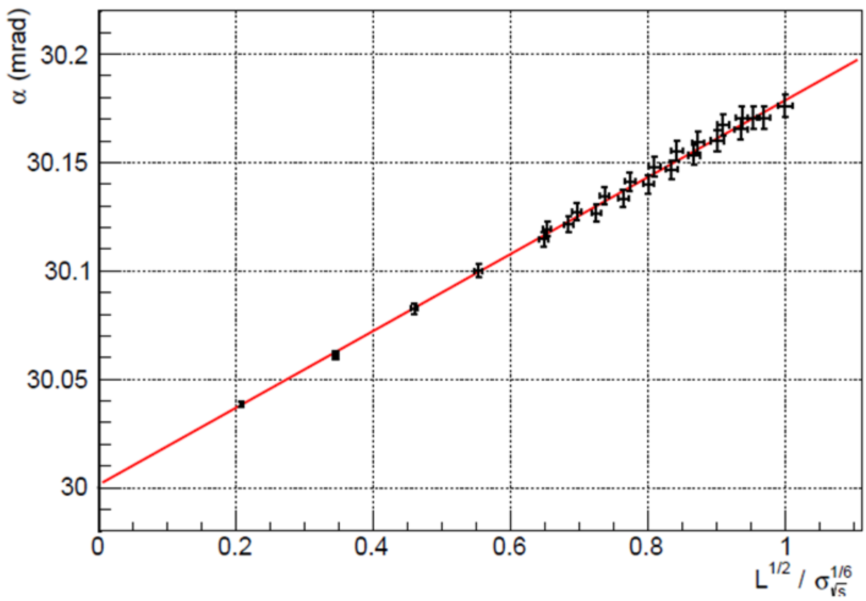

Fig. 125: Change in the measured crossing-angle α plotted against $\mathcal{L}^{1/2}/\sigma_{\mathrm{E_{CM}}}{}^{1/6}$ (see main text), at various points during the top-up injection. Extrapolation down to $\mathcal{L}^{1/2}/\sigma_{\mathrm{E_{CM}}}{}^{1/6} = 0$ allows the crossing-angle to be determined in the absence of bunch-bunch effects [18].

The longitudinal boost and the collision-energy spread

The dimuon topology allows the longitudinal boost to be determined on an event-by-event basis. When averaged over a suitable sample size, this provides valuable information for understanding the energy loss around the ring, and calculating the local collision energy at each interaction point. The width of this distribution (see Fig. 126) is a measure of $\sigma_{E_{CM}}$,which is an essential input to measurements such as the Z and W width. Again, the foreseen statistical precision on these quantities is excellent. For example, the energy spread can be measured to one part in a thousand with one million dimuon events. Recent work has investigated how sensitive the determination of $\sigma_{E_{CM}}$ is to the knowledge of the ISR corrections in the dimuon production. The conclusion is that the measurement is robust; even if it is assumed that the second-order corrections from initial-state radiation (ISR) are unknown, the resulting bias on the extraction of $\sigma_{E_{CM}}$ is far smaller than the statistical uncertainty.

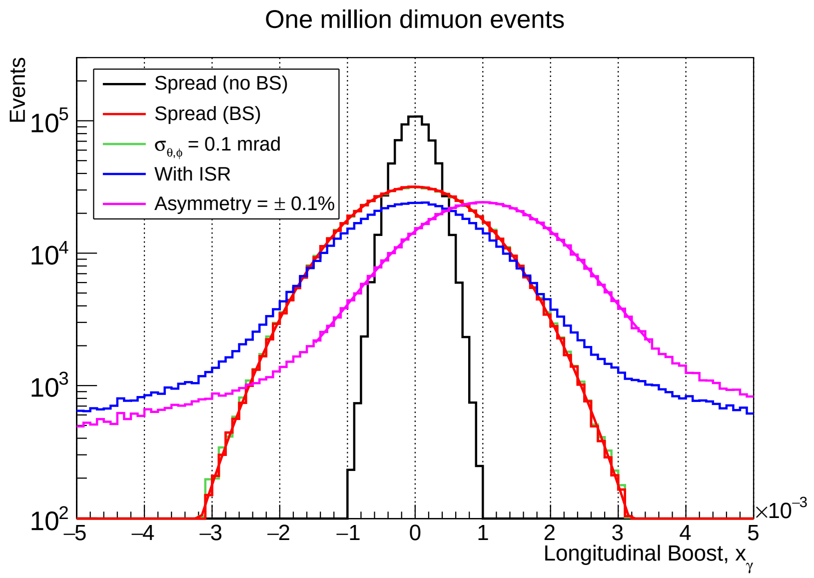

Fig. 126: Fitted value of longitudinal boost from one million muon-pair events at one of the FCC-ee IPs [18]. Once the ISR is unfolded this can be used to measure the energy spread. The magenta line shows the impact of a centre-of-mass boost on the distribution. The shift can be measured with a statistical precision of 40 keV.

Relative E_{CM} *determination*

The reconstructed peak position of the dimuon invariant-mass distribution provides an excellent proxy for the collision energy. The difference in this reconstructed position between the points of the Z-resonance scan provides a measure of the change in collision energy, which is a critical input for several analyses, in particular the measurement of the Z width. The distribution is fit in bins of the polar angle for back-to-back events. An example fit is shown in Fig. 127 (left). The statistical precision on this pseudo-E_{CM} measurement, when summing the samples from four experiments, is around 20 keV for each of the two off-peak running points, assuming the momentum resolution of the IDEA detector.

In order for the detector not to introduce a bias in this measurement larger than the statistical precision, the momentum scale must be controlled at this level. The field stability can be tracked with NMR probes, and the momentum scale directly monitored through the reconstruction of low-mass resonances. However, even with a perfect detector there is a bias in the pseudo-E_{CM} measurement in the Z scan that arises from ISR/FSR effects, and the product of the Breit-Wigner shape of the resonance and the Gaussian distribution of the energy spread of the colliding beams. The value of this bias differs by about 8 MeV when going from $E_{CM} = 87.9$ GeV to 94.3 GeV, as can be seen in Fig. 127 (right). This difference must be corrected for in the measurement, which necessitates a good understanding of the effect of ISR/FSR. In a generator-level study, disabling ISR/FSR changes the difference in the bias between the two off-peak points by around 500 keV. Thus control of these ISR/FSR effects to the 1% level would be sufficient to render their impact negligible for the Z-width measurement.

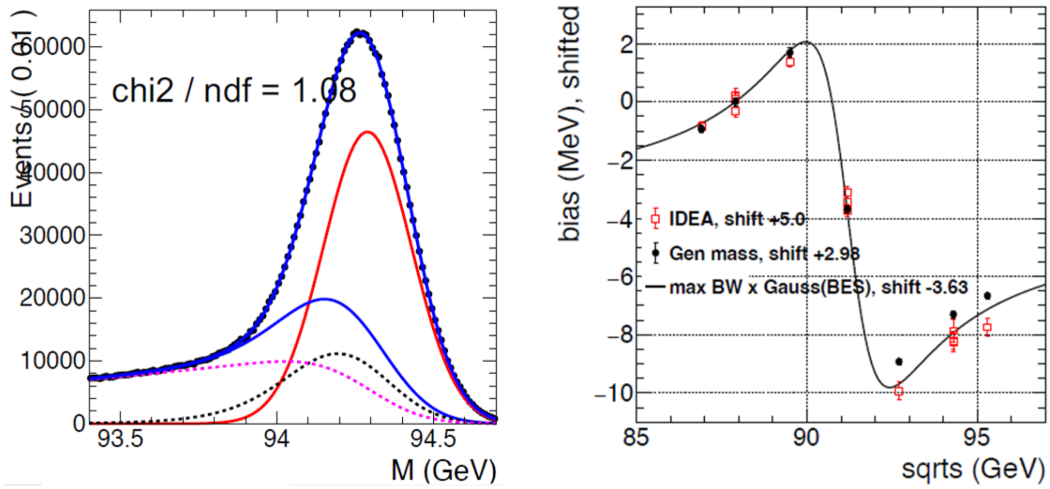

Fig. 127: Left: an example fit to the dimuon invariant-mass distribution at $\mathrm{E_{CM}} = 94.3$ GeV. Right: the bias between the $\mathrm{E_{CM}}$ as determined from the dimuon invariant-mass fit and the true value. Results are shown for the simulated performance of the IDEA detector (red points), the expected dependence with ISR/FSR included (black points), and the expected dependence with ISR/FSR effects disabled (black curve). A single shift (a few MeV in all cases) has been applied to each set of results, so that the bias for all is zero at 87.9 GeV. *Figure to be updated*

Absolute $\mathrm{E_{CM}}$ *determination*

At collision energies above the Z, the dimuon events may be used to provide an absolute measurement of $\mathrm{E_{CM}}$. Radiative returns, in which the emission of an initial-state photon means that the dimuon pair has an invariant mass of the Z, allows for calibration of events where there is no ISR. The method can be extended to include multihadron final states also. This method is of great value for physics studies in the regime where no RDP is possible, *i.e.* collision energies above 200 GeV. This approach also provides a useful complementary measure of $\mathrm{E_{CM}}$ in the intermediate energies where RDP is possible but challenging. The foreseen statistical precision is around 280 keV for 6 $\mathrm{ab^{-1}}$ of integrated luminosity at $\mathrm{E_{CM}} = 125$ GeV and 340 keV for 12 $\mathrm{ab^{-1}}$ at $\mathrm{E_{CM}} = 160$ GeV.

8.3 Expected precision on the electroweak observables from the measurement of the collision energy and collision-energy spread

Several of the most important electroweak observables are expected to have a dominant or significant systematic uncertainty associated with the knowledge of the collision energy and collision-energy spread. The collision-energy uncertainties can be classed in three distinct categories, itemised below. These uncertainties propagate to the physics results in an observable-dependent manner, as discussed in Ref. [18].

- Uncertainties that are fully correlated between measurements propagate to the knowledge of the absolute energy scale. Examples include the values of $g-2$ and the mass of the electron, the RF frequency scale, and any other systematic bias that occurs at all times and at all energies. At this stage in the studies it is estimated that this uncertainty will be around 100 keV on the collision energy at the Z pole, and 300 keV at the $\mathrm{W^+W^-}$ threshold. This contribution is expected to be the dominant systematic uncertainty in the measurements of the Z and W mass.
- A point-to-point contribution comprises biases that occur at all times, or lead to an average shift, but are different for each energy setting. The principal method of determining this uncertainty will be from the invariant mass of dimuons, as reconstructed by the experiments. The estimated size of this uncorrelated uncertainty is 20 keV for each off-peak point of the Z-resonance scan. The understanding gained at the Z pole and complementary measurements will lead to a corresponding

Table 22: Current projected E_{CM}-related uncertainties on selected electroweak observables.

Uncertainty	Observable				
	m_Z [keV]	Γ_Z [keV]	$\sin^2\theta_W^{eff}$ [$\times 10^{-6}$]	$\frac{\Delta\alpha_{QED}(m_Z^2)}{\alpha_{QED}(m_Z^2)}$ [$\times 10^{-5}$]	m_W [keV]
Absolute	100	2.5	/	0.1	150
Point-to-point	14	11	1.2	0.5	50
Sample size	1	1	0.1	/	3
Energy spread	/	10	/	0.1	/
Total E_{CM} related	101	15	1.2	0.5	158
FCC-ee statistical	4	4	2	3	250

uncertainty of around 100 keV at the W^+W^- threshold. The point-to-point uncertainty is expected to be the dominant contribution in the measurement of the Z width.

– The uncertainty on each individual RDP measurement is dominated by an uncertainty that is set by the frequency of the polarimeter sampling or the size of the energy bins in which the depolarisation can be located. A reasonable estimate of this uncertainty is 200 keV at the Z pole and 300 keV at the W^+W^- threshold. As this component is statistical in nature, its impact decreases with the square-root of the sample size of measurements. As it is planned to collect $\sim 10^4$ measurements at each energy point the final uncertainty from this source will be essentially negligible compared to other contributions. However, the importance of making each measurement as precise as possible, and collecting the largest possible number of measurements, will become more evident when the data set is split into smaller samples for performing systematic checks.

The contributions from each category of uncertainty, and their quadratic sum, are listed in Table 22 for several key electroweak observables.

Also shown in Table 22 is the contribution from the uncertainty in the knowledge of the energy spread, which affects quantities with a strong quadratic dependence on the collision energy. Observables that are most susceptible to this uncertainty include the Z-peak cross section and the Z width. Assuming a collision-energy spread of 85 MeV, determined with a precision of ± 0.05 MeV, leads to a sub-dominant systematic uncertainty in the measurement of these observables.

It can be seen that with current expectations it will be possible to reduce the uncertainty from energy-related quantities by an order of magnitude or better with respect to what was achieved at LEP. The entries in Table 22 for the E_{CM}-related systematic uncertainty can be compared to the corresponding LEP values of 1.7 MeV for m_Z, 1.2 MeV for Γ_Z and 9 MeV for m_W. With further studies it is hoped that these uncertainties can be reduced still further. It is noted that this systematic is only limiting in the measurement of m_Z and Γ_Z. In the latter case improvements in the point-to-point and energy-spread contributions may allow this conclusion to be revised.

8.4 Prospects for monochromatisation and the measurement of the electron Yukawa

Author: David d'Enterria

The electron Yukawa via resonant Higgs production $e^+e^- \to$ H at 125 GeV

Confirming the mechanism of mass generation for the stable visible elementary particles of the universe, composed of u and d quarks plus the electron (and neutrinos), is experimentally very challenging because of the low masses of the first-generation fermions and thereby their small Yukawa couplings to the Higgs field (the neutrino mass generation remains a BSM problem in itself). In the SM, the Yukawa coupling of the electron is $y_{\rm e} = \sqrt{2}m_{\rm e}/v = 2.8\cdot10^{-6}$ for $m_{\rm e}(m_{\rm H}) = 0.486\cdot10^{-3}\,$GeV and Higgs vacuum expectation value $v = (\sqrt{2}{\rm G_F})^{-1/2} = 246.22\,$GeV, and measuring it via $\rm H\to e^+e^-$ appears hopeless at hadron colliders because the decay has a tiny partial width due to its dependence on the $\rm e^\pm$ mass squared:

$$\Gamma({\rm H\to e^+e^-}) = \frac{\rm G_F m_H m_e^2}{4\sqrt{2}\,\pi}\left(1-\frac{4\,\rm m_e^2}{\rm m_H^2}\right)^{3/2} = 2.14\cdot10^{-11}{\rm GeV}\,, \tag{9}$$

which corresponds to a $\mathcal{B}(\rm H\to e^+e^-)\approx 5\cdot10^{-9}$ branching fraction for the SM Higgs boson with $m_{\rm H} = 125\,$GeV mass and $\Gamma_{\rm H} = 4.1\,$MeV total width. At the LHC and FCC-hh, such a final state is completely swamped by the Drell–Yan $\rm e^+e^-$ continuum whose cross section is many orders of magnitude larger. The first LHC searches with about 20 $\rm fb^{-1}$ of p-p collisions at 8 TeV, assuming the SM Higgs production cross section, lead to an upper bound on the branching fraction of $\mathcal{B}(\rm H\to e^+e^-) < 1.9\cdot10^{-3}$ at 95% confidence level (CL), corresponding to an upper limit on the Yukawa coupling $y_{\rm e}\propto\mathcal{B}(\rm H\to e^+e^-)^{1/2}$ of 600 times the SM value [702]. Such results were further updated in [703, 704], exploiting about 140 $\rm fb^{-1}$ of pp data at $\sqrt{s} = 13$ TeV and reaching an observed upper limit of $\mathcal{B}(\rm H\to e^+e^-) < 3.0\times10^{-4}$ at 95% CL. This latter value translates into a current upper bound on the Higgs boson effective coupling modifier to electrons of $|\kappa_{\rm e}| < 240$. Assuming that the sensitivity to the $\rm H\to e^+e^-$ decay scales simply with the square root of the integrated luminosity, the HL-LHC phase with a $\mathcal{L}_{\rm int} = 2\times3\,{\rm ab}^{-1}$ data sample (combining ATLAS and CMS results) will result in $y_{\rm e}\lesssim 100y_{\rm e}^{\rm SM}$. Based on searches for the similar $\rm H\to\mu^+\mu^-$ channel, one can expect upper limits on $\mathcal{B}(\rm H\to e^+e^-)$ to be further improved by factors of about four by adding more Higgs production categories and using advanced multivariate analysis methods, eventually reaching $y_{\rm e}\lesssim 50y_{\rm e}^{\rm SM}$ at the end of the HL-LHC.

About ten years ago, it was first noticed that the unparalleled integrated luminosities of $\mathcal{L}_{\rm int}\approx 10\,{\rm ab}^{-1}$/year expected at $\sqrt{s} = 125\,$GeV at the FCC-ee would make it possible to attempt an observation of the direct production of the scalar boson and thereby directly measure the electron Yukawa coupling [705, 706]. Subsequently, various theoretical [22, 707–710], simulated data analysis [24], and accelerator [711–713] works discussed different aspects of the $\rm e^+e^-\to H$ measurement. The Feynman diagrams for s-channel Higgs production (and its most statistically significant decay, see below) and dominant backgrounds are shown in Fig. 128 (left). The resonant Higgs cross section in $\rm e^+e^-$ collisions at a given CM energy $\sqrt{s}$ is theoretically given by the relativistic Breit–Wigner (BW) expression:

$$\sigma_{\rm ee\to H} = \frac{4\pi\Gamma_{\rm H}\Gamma({\rm H\to e^+e^-})}{(s-m_{\rm H}^2)^2+m_{\rm H}^2\Gamma_{\rm H}^2}. \tag{10}$$

From this expression, it is first clear that an accurate knowledge of the value of $m_{\rm H}$ is critical to maximize the resonant cross section. Combining three $\rm e^+e^-\to HZ$ measurements at FCC-ee (recoil mass, peak cross section, and threshold scan), a $\mathcal{O}(2\,{\rm MeV})$ mass precision is achievable [27] before any dedicated $\rm e^+e^-\to H$ run. In addition, the FCC-ee beam energies will be monitored with a relative precision of 10^{-6} [19], providing a sub-MeV accuracy on the exact point in the Higgs lineshape being probed at any moment. For $m_{\rm H} = 125\,$GeV, Eq. (10) gives $\sigma_{\rm ee\to H} = 4\pi\mathcal{B}({\rm H\to e^+e^-})/{\rm m_H^2} = 1.64$ fb as peak cross section. Two effects, however, lead to a significant reduction of the Born-level result: (i) initial-state γ radiation (ISR) depletes the cross section and generates an asymmetry of the Higgs lineshape, and (ii) the actual beams are never perfectly monoenergetic, i.e., the collision $\sqrt{s}$ has a spread $\delta_{\sqrt{s}}$ around its central value[29], further leading to a smearing of the BW peak. For FCC-ee operating at 125 GeV, the natural spread in collision energy due to synchrotron radiation will be around 50 MeV, rising to 70 MeV through the effects of beamstrahlung. The reduction of the BW cross section due to IS photon emission(s) is of factor of 0.35 and leads to $\sigma_{\rm ee\to H} = 0.57$ fb [707]. The additional impact of a given CM energy spread on the Higgs BW shape can be quantified through the convolution of BW and Gaussian distributions, i.e., a relativistic Voigtian function. Figure 128 (right) shows the Higgs lineshape for various $\delta_{\sqrt{s}}$ values. The

[29] This energy spread is the same quantity denoted $\sigma_{\rm E_{CM}}$ elsewhere in Sec. 8.

combination of ISR plus $\delta_{\sqrt{s}} = \Gamma_\mathrm{H} = 4.1\,\mathrm{MeV}$ reduces the peak Higgs cross section by a total factor of 0.17, down to $\sigma_{\mathrm{ee}\to\mathrm{H}} = 0.28$ fb. Though tiny, the cross section for any other $\mathrm{e^+e^-} \to \mathrm{H}$ production process, through W and Z loops, is further suppressed by the electron mass for on-shell external fermions (chirality flip) and is negligible [23].

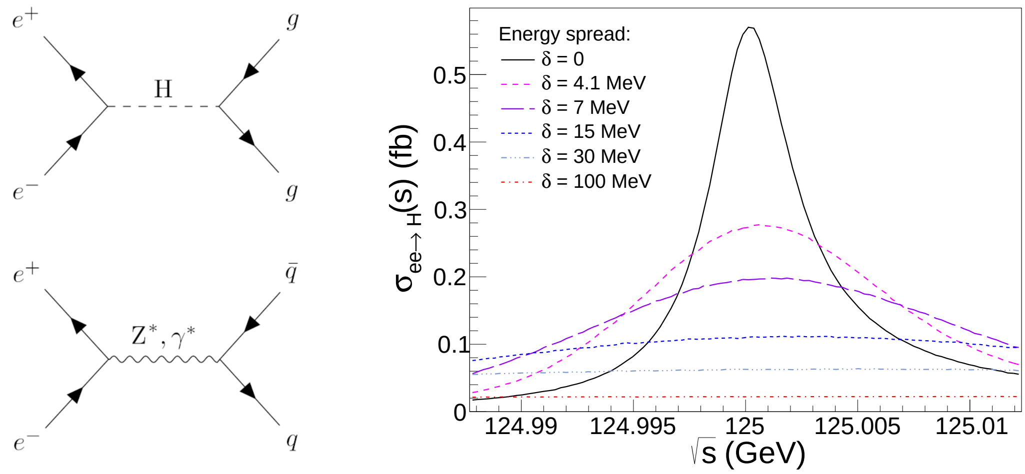

Fig. 128: Left: Diagrams for the s-channel production of the Higgs boson decaying into two gluon jets (upper) and reducible Z^* quark dijet backgrounds (lower) in $\mathrm{e^+e^-}$ at $\sqrt{s} = 125$ GeV. Right: Resonant Higgs production cross section at $\sqrt{s} = 125$ GeV, including ISR effects, for several $\mathrm{e^+e^-}$ CM energy spread values: $\delta_{\sqrt{s}}$ = 0, 4.1, 7, 15, 30, and 100 MeV [707].

The three main challenges of the $\mathrm{e^+e^-} \to \mathrm{H}$ measurement have been discussed in Ref. [24]: (i) the need to know accurately ($\mathcal{O}(\mathrm{MeV})$) beforehand the value of the Higgs boson mass where to operate the collider, (ii) the smallness of the resonant cross section (few hundred ab) due to ISR and the collision-energy spread ($\delta_{\sqrt{s}}$) that requires monochromatisation of the beams, i.e., to reduce $\delta_{\sqrt{s}}$ to the few MeV scale, while still delivering large (few ab^{-1}) integrated luminosities $\mathcal{L}_\mathrm{int}$, and (iii) the existence of multiple backgrounds with orders-of-magnitude larger cross section than the Higgs signal decay channels themselves. As mentioned above, the knowledge of m_H with a few MeV accuracy seems feasible at FCC-ee [27]. The latest developments of the monochromatisation schemes at FCC-ee, point (ii), are summarized below. The challenge (iii) has been addressed in detail in Ref. [24] where a generator-level study was performed choosing a benchmark monochromatisation point leading to $(\delta_{\sqrt{s}}, \mathcal{L}_\mathrm{int}) = (4.1\,\mathrm{MeV}, 10\,\mathrm{ab}^{-1})$, corresponding to a peak s-channel cross section of $\sigma_{\mathrm{e^+e^-}\to\mathrm{H}} = 280\,\mathrm{ab}$, and 2 800 Higgs bosons produced. The strategy to observe the resonant production of the Higgs boson is based on identifying final states consistent with any of the H decay modes, that lead to a small excess (but, hopefully, statistically significant when combined together) of the measured cross sections with respect to the theoretical expectation for their occurrence via background processes alone, involving Z^*, γ^*, or t-channel exchanges. For this purpose, large simulated event samples of signal and associated backgrounds have been generated with the PYTHIA 8 Monte Carlo (MC) code [714] for 11 Higgs boson decay channels. A simplified description of the expected experimental performances has been assumed for the reconstruction and (mis)tagging of heavy-quark (c, b) and light-quark and gluons (udsg) jets, photons, electrons, and hadronically decaying tau leptons. Generic preselection criteria have been defined targeting 11 Higgs boson channels, suppressing reducible backgrounds while keeping the largest fraction of the signal events. A subsequent multivariate analysis of $\mathcal{O}(50)$ kinematic and global topological variables, defined for each event, has been carried out. Boosted-Decision-Trees (BDT) classifiers have been trained on signal and background events, to maximize the signal significances for each individual channel. The most significant Higgs decay channels are found to be $\mathrm{H} \to \mathrm{gg}$ (for a gluon efficiency of 70% and a uds-for-g jet mistagging rate of 1%), and $\mathrm{H} \to \mathrm{WW}^* \to \ell\nu\,jj$. The digluon final state is the most sensitive channel to search for the resonant Higgs boson production (Fig. 128 left, upper) because it possesses a moderately large branching fraction ($\mathcal{B} \approx 8\%$) while the irreducible $Z^* \to gg$ background is forbidden by the Landau–Yang theorem. The most important experimental challenge is to reduce the light-quark for gluon mistagging rate to the 1% level (while keeping the efficiency for the $H \to gg$ channel at 70%) to keep the overwhelming $Z^* \to u\bar{u}, d\bar{d}, s\bar{s}$ backgrounds (Fig. 128 left, lower) under control. Such a mistagging rate is a factor of about seven times better than the current state-of-the-art for jet-flavour tagging algorithms [444], but it is a realistic goal given all the experimental and theoretical improvements in our understanding of parton radiation and hadronization expected at the FCC-ee [715].

Combining all results for an accelerator operating at $(\delta_{\sqrt{s}}, \mathcal{L}_{\rm int}) = (4.1\,\text{MeV}, 10\,\text{ab}^{-1})$, a 1.3σ signal significance can be reached for the direct production of the Higgs boson, corresponding to an upper limit on the electron Yukawa coupling at 1.6 times the SM value: $|y_e| < 1.6|y_e^{\rm SM}|$ at 95% confidence level (CL), per FCC-ee interaction point (IP) and per year. Based on this benchmark result and the parametrised dependence of the resonant Higgs cross section on $\delta_{\sqrt{s}}$ (Fig. 128, right), bidimensional maps of $e^+e^- \to H$ significances and electron-Yukawa sensitivities have been determined in the $(\delta_{\sqrt{s}}, \mathcal{L}_{\rm int})$ plane. Figure 129 shows the 95% CL upper limit contours on the electron Yukawa coupling strength as a function of the energy spread and integrated luminosity with the red star (on the red-dashed line corresponding to a reference monochromatised collision-energy spread equal to the Higgs boson width) indicating the result of this benchmark study.

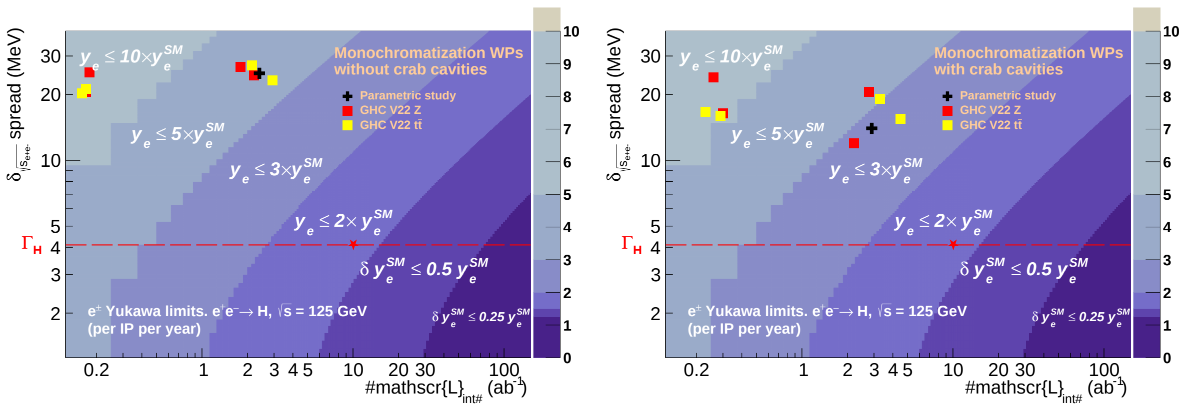

Fig. 129: Upper limits contours (95% CL) on the electron Yukawa y_e in the CM-energy-spread $\delta_{\sqrt{s}}$ vs. integrated-luminosity $\mathcal{L}_{\rm int}$ plane, without (left) and with (right) crab cavities. The red star over the $\delta_{\sqrt{s}} = \Gamma_H = 4.1\,\text{MeV}$ red-dashed line, indicates the reference point assumed in the physics simulation analysis [24]. The black cross indicates the previously achieved working point with self-consistent parametric monochromatisation [713, 716]. The red and yellow squares indicate the monochromatisation points based on simulations of the "GHC V22 Z" and "GHC V22 $\bar{t}t$" optics, respectively [717].

FCC-ee monochromatisation

Monochromatisation is necessary to reduce $\delta_{\sqrt{s}}$ to the few-MeV level of the natural SM Higgs width and thereby increase the sensitivity of the electron-Yukawa measurement. It is a strategy first proposed around 50 years ago [718], and relies on creating opposite correlations between spatial position and energy deviations within the colliding beams with nominal beam energy (E_0). Figure 130 shows a schematic of the principle of monochromatisation for beams that collide head on and for those that collide with a crossing angle (θ_C). The current baseline design of FCC-ee corresponds to the crossing-angle configuration, as it is not foreseen to deploy crab cavities. In both configurations, the correlations between transverse (either horizontal or vertical) position in the beam and energy lead to a spread in collision energy that is lower than in the uncorrelated case.

Monochromatisation can be achieved by adding dedicated components at the interaction region

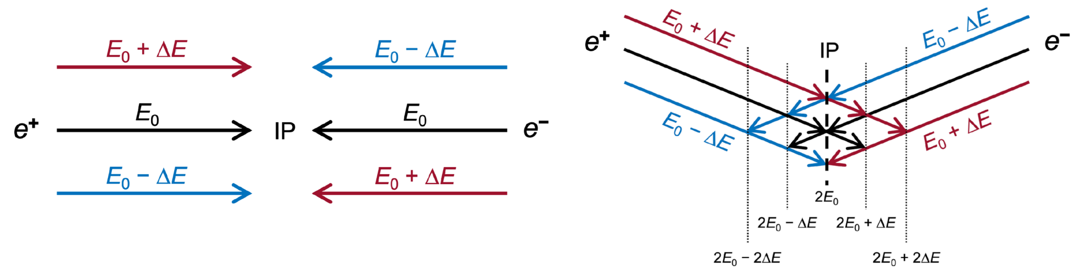

Fig. 130: Schematic of the principle of monochromatisation shown for head-on collisions (left) and for collisions with a crossing angle (right). In both cases opposite-sign correlations between the transverse position in the beam and energy lead to a reduction in the spread of collision energy compared with the uncorrelated case.

(IR) to generate a non-zero dispersion function with opposite signs for the two beams at the IP. A non-zero dispersion function at the IP in the horizontal and/or vertical directions ($D^*_{x,y} \neq 0$) enlarges the IP transverse beam size ($\sigma^*_{x,y}$) which in turn affects the luminosity, $\mathcal{L} \propto 1/(\sigma^*_x \sigma^*_y)$. The monochromatisation factor (λ) is defined as:

$$\lambda = \sqrt{1 + \sigma_\delta^2 \left(\frac{D_x^{*2}}{\varepsilon_x \beta_x^*} + \frac{D_y^{*2}}{\varepsilon_y \beta_y^*} \right)} \tag{11}$$

with σ_δ the relative energy spread, $\varepsilon_{x,y}$ the transverse emittances and $\beta^*_{x,y}$ the betatron functions at the IP. For any value of λ achieved, the $\delta_{\sqrt{s}}$ and the $\mathcal{L}$ in the monochromatisation operation mode are given by:

$$\delta_{\sqrt{s}} = \frac{\sqrt{2} E_0 \sigma_\delta}{\lambda} \quad \text{and} \quad \mathcal{L} = \frac{\mathcal{L}_0}{\lambda} , \tag{12}$$

where $\mathcal{L}_0$ represents the luminosity for the same values of $\beta^*_{x,y}$ but without $D^*_{x,y}$. Consequently, the design of a monochromatisation scheme requires considering both the IR beam optics and the optimization of other collider parameters to maintain the highest possible luminosity. Possible approaches to monochromatisation for FCC-ee have been studied for several years, starting from self-consistent parametric studies [711, 713, 716, 719]. Recent developments [717, 720] comprise a detailed study of the IP-region optics required for monochromatisation, exploring different potential configurations and their implementation in the FCC-ee global lattice, along with beam-dynamics simulations and performance evaluations including the impact of beamstrahlung (BS).

The baseline FCC-ee standard lattice design is the so-called 'Global Hybrid Correction' (GHC) optics [569, 721, 722]. It allows for four experimental IRs where the e^+ and e^- beams are brought to collision from the inside outwards with a $\theta_c = 30$ mrad angle in the horizontal plane and a virtual vertical crab-waist scheme. Here presented monochromatisation studies are based on, two versions of this optics: "FCC-ee GHC V22 Z", where the lattice is optimised for operation at the Z pole, and "FCC-ee GHC V22 $t\bar{t}$", which is optimised for operation above the $t\bar{t}$ threshold (in both 'V22' designates the 2022 configuration).

Three approaches to monochromatisation have been investigated. In the first, the horizontal dipoles used for the local-chromaticity-correction system are reconfigured to generate a non-zero D^*_x of size ~ 10 cm, while maintaining the same θ_C. Given the values of the other parameters in Eq. (11) [721] it follows that monochromatisation factors of $\lambda = 5$–8 are achievable. This study was performed both to provide monochromatisation in all four IRs and then repeated to give monochromatisation in two IRs only. The second method introduces a non-zero value of D^*_y by adjusting the strengths of the skew quadrupoles in the interaction region. The very low vertical emittance in FCC-ee, means that similar monochromatisation factors as in the horizontal case can be achieved with $D^*_y \sim 1$ mm. Finally, schemes involving non-zero values of both D^*_x and D^*_y have been explored. In all cases, the layout of the components around the IR and the parameter values were adjusted to satisfy the boundary conditions in the machine and deliver optimum performance.

Guinea-Pig simulations [574] were performed to determine the performance of the different monochromatisation schemes, taking into account the impact of BS. The particle distribution at the IP was simulated as an ideal Gaussian distribution, comprising 40,000 particles, and defined by the following global optical performance parameters: E_0, σ_δ, $\varepsilon_{x,y}$, $\beta^*_{x,y}$, $D^*_{x,y}$, σ_z, and θ_c. For each configuration, the $\delta_{\sqrt{s}}$ (from the distribution of the CM energy) and $\mathcal{L}$ were calculated. The results are presented in Tables 23 and 24 for the 'GHC V22 Z' and 'GHC V22 $t\bar{t}$ optics, respectively.

Table 23: Values of $\delta_{\sqrt{s}}$, $\mathcal{L}$, and $\mathcal{L}_{\text{int}}$ for various setups of the 'FCC-ee GHC V22 Z' monochromatisation IR optics [717]. 'Std. ZES' refers to the layout without monochromatisation, 'ZH4IP' ('ZH2IP') refers to the layout with $D^*_x \neq 0$ in four (two) IPs, 'ZV' refers to the layout with $D^*_y \neq 0$, and 'ZHV' refers to the layout with $D^*_{x,y} \neq 0$.

Parameter [Unit]	Std. ZES	ZH4IP	ZH2IP	ZV	ZHV
CM energy spread $\delta_{\sqrt{s}}$ [MeV]	69.52	26.80	24.40	25.25	20.58
Luminosity / IP $\mathcal{L}$ [10^{34} cm^{-2}s^{-1}]	44.8	15.0	18.4	1.46	1.42
Integrated luminosity / IP / year $\mathcal{L}_{\text{int}}$ [ab^{-1}]	5.38	1.80	2.21	0.18	0.17

Table 24: Values of $\delta_{\sqrt{s}}$, $\mathcal{L}$, and $\mathcal{L}_{\text{int}}$ for various setups of the "FCC-ee GHC V22 $\bar{\text{t}}$t" monochromatisation IR optics [717]. 'Std. TES' refers to the layout without monochromatisation, 'TH4IP' ('TH2IP') refers to the layout with $D^*_x \neq 0$ in four (two) IPs, 'TV' refers to the layout with $D^*_y \neq 0$, and 'THV' refers to the layout with $D^*_{x,y} \neq 0$.

Parameter [Unit]	Std. TES	TH4IP	TH2IP	TV	THV
CM energy spread $\delta_{\sqrt{s}}$ [MeV]	67.20	27.10	23.16	20.23	21.24
Luminosity / IP $\mathcal{L}$ [10^{34} cm^{-2}s^{-1}]	71.2	17.9	24.5	1.37	1.42
Integrated luminosity / IP / year $\mathcal{L}_{\text{int}}$ [ab^{-1}]	8.54	2.15	2.94	0.16	0.17

All of the monochromatisation schemes investigated are successful in reducing $\sigma_{\sqrt{s}}$ by a factor or two or more with respect to the value without monochromatisation. As expected, this reduction in energy spread is accompanied by a reduction in luminosity, which is more marked for the configurations with $D^*_y \neq 0$ and combined $D^*_{x,y} \neq 0$, where the BS leads to a blow up in ϵ_y. The corresponding physics performances are plotted as red (yellow) squares for the "GHC V22 Z" ("GHC V22 $\bar{\text{t}}$t") setups in the ($\delta_{\sqrt{s}}$, $\mathcal{L}_{\text{int}}$) plane in Fig. 129 (left), from which the corresponding 95% CL upper limits contours for the y_{e} coupling can be read off. The results without crab cavities are shown in Fig. 129 (left). The physics performances of all designed monochromatisation IR optics with nonzero D^*_x are comparable to or even exceed those of the previous FCC-ee self-consistent parameters (black cross). The "MonochroM TH2IP" optics achieves the best $\delta_{\sqrt{s}}$ vs. $\mathcal{L}_{\text{int}}$ benchmark, with $\delta_{\sqrt{s}} = 23.16$ MeV and $\mathcal{L}_{\text{int}} = 2.94$ ab^{-1}. This corresponds to an upper limit (95% CL) of $|y_{\text{e}}| < 3.2\,|y_{\text{e}}^{SM}|$ for the Higgs-electron coupling, per IP per year. With the same analysis under the head-on collision configuration including crab cavities, the physics performances of all proposed monochromatisation schemes are further improved [720], as shown in Fig. 129 (right). The best $\delta_{\sqrt{s}}$ vs. $\mathcal{L}_{\text{int}}$, achieved with the "MonochroM TH2IP" optics, yielding $\delta_{\sqrt{s}} = 15.46$ MeV and $\mathcal{L}_{\text{int}} = 4.51$ ab^{-1}, indicates an upper limit of $|y_{\text{e}}| < 2.6\,|y_{\text{e}}^{SM}|$.

Since the 95% CL upper limit on the $\text{e}^+\text{e}^- \to \text{H}$ production cross section scales as $\sqrt{\mathcal{L}_{\text{int}}^{-1}}$, and the cross section scales as y_{e}^2, the upper limits on the electron Yukawa improve as $\propto \sqrt{\mathcal{L}_{\text{int}}^{-1/4}}$. For four experiments running with the same luminosity at different IPs with the 'TH4IP' scheme in the 'GHC V22 $t\bar{t}$ optics with crossing angle, one would set an upper limit (95% CL) of about xx times the SM value in one year of operation. This is to be compared with yy times the SM value when operating without monochromatisation.

8.5 Future studies

The studies performed before and during the Feasibility Study have established a baseline scheme for calibration of the collision energy that will ensure the physics goals of FCC-ee can be met. Nevertheless, these studies must be refined in certain areas, and alternative approaches should be considered that will further improve the performance.

The measurements of energy-related quantities made by the experiments using dimuon events are a critical ingredient in the $\mathrm{E_{CM}}$ calibration. Recently, several of these studies have been deepened to validate their robustness against the uncertainties in the knowledge of higher-order ISR/FSR effects. This work will be extended. The impact of detector performance and the interplay with alignment studies will be another focus of attention. Finally, the use of other categories of physics events, beyond dimuons, will be investigated.

It is important to have a solid strategy to translate from the mean beam energy to the local collision energy at each interaction point. This will be done using the measurement of the longitudinal boosts at the experiment and from knowledge and related studies of the impedances in the machine. Full simulations of this procedure will be conducted. Attention will also be paid to the control of energy shifts from possible dispersion effects at each interaction point, and the requirements that this places on the system of beam-position monitors.

More detailed simulations of the level and lifetime of transverse polarisation will be performed, in parallel with any evolution in the proposed optics of the accelerator. A deeper understanding will be sought of any effects that bias the assumed proportionality between the spin tune and mean beam energy. It will be particularly important to monitor the expected level of polarisation at the $\mathrm{W^+W^-}$ threshold and the RDP strategy in this challenging regime. Detailed technical designs will be made of the polarimeter and depolariser systems.

The current baseline strategy is to inject unpolarised beams and to stimulate the growth of polarisation in the pilot bunches by activating the wigglers at start of fill. This is a robust approach, but introduces dead-time when no collisions are possible. Effort will therefore be given to investigating the possibility of injecting pilot bunches that have already been polarised. For this to be feasible, the design of the injection system must be modified and simulations will be required to validate that the bunches retain their polarisation throughout injection and in the booster ring.

The studies on feasibility of measuring the electron Yukawa will continue. On the accelerator side, new and refined schemes for improving the energy monochromatisation will be investigated. It will also be necessary to develop and simulate a procedure to monitor and adjust the collision energy in real time, to ensure that the operation remains centred at the Higgs pole. Physics studies will continue to improve the signal yield and signal-to-background discrimination. It has been noted that without crab cavities the foreseen performance is worse, but correlations exist between the monochromatisation and the longitudinal coordinate of the collision. With this in mind, it will be investigated whether performance can be regained by performing a differential measurement accounting for this correlation.

9 Community building

An important aspect for the success of the FCC project is the strength of the global community, which eventually will split into several (probably four) experimental collaborations and an accelerator team. This splitting is not expected to happen before a decision to move forward with the project is taken by the CERN council (2028 ?), however community building takes time, so the FCC collaboration is giving high priority to this enterprise.

The FCC project is built on six pillars (Accelerators, Physics-Experiments-Detectors, Technical